Tracking Glioma Evolution in human brain for precision medicine by integrating real-time in vivo tumour genomes

Xingyao Bu (xingyaob@zzu.edu.cn)
Zhengzhou University People's Hospital, Henan University People's Hospital

Kaiyuan Deng
Zhengzhou University People's Hospital, Henan University People's Hospital

Zhiyuan Sheng
Zhengzhou University People's Hospital, Henan University People's Hospital

Sensen Xu
Zhengzhou University People's Hospital, Henan University People's Hospital

Yage Bu
Zhengzhou University People's Hospital, Henan University People's Hospital

Shuang Wu
Zhengzhou University People's Hospital, Henan University People's Hospital

Ziyue Zhang
Zhengzhou University People's Hospital, Henan University People's Hospital

Guangzhong Guo
Zhengzhou University People's Hospital, Henan University People's Hospital

Guanzheng Liu
Zhengzhou University People's Hospital, Henan University People's Hospital

Jinliang Yu
Zhengzhou University People's Hospital, Henan University People's Hospital

Yushuai Gao
Zhengzhou University People's Hospital, Henan University People's Hospital

Zhaoyue Yan
Zhengzhou University People's Hospital, Henan University People's Hospital

Chaojie Bu
Zhengzhou University People's Hospital, Henan University People's Hospital

Jianjun Gu
Zhengzhou University People's Hospital, Henan University People's Hospital

Lingfei Kong
Zhengzhou University People's Hospital, Henan University People's Hospital

Gang Liu

Zhengzhou University People's Hospital, Henan University People's Hospital

Meiyun Wang

Zhengzhou University People's Hospital, Henan University People's Hospital

Tianxiao Li

Zhengzhou University People's Hospital, Henan University People's Hospital

---

Research Article

Keywords: glioma, temozolomide, clone evolution, precision medicine, tumor in situ fluid, liquid biopsy

Posted Date: April 18th, 2022

DOI: https://doi.org/10.21203/rs.3.rs-1550999/v1

Abstract

Background: Targeted therapy of glioma is unsatisfactory due to the variable heterogeneity of tumors. We tracked glioma genomic alterations in vivo to provide a boost to precision medicine.

Methods: We collected tumor tissue samples from glioma patients (including recurrent tumors) and serially collected Tumor in situ fluid (TISF) after surgery. Glioma-derived DNA from these samples was sequencing by next-generation DNA sequencing. We longitudinally analysed the genomes of glioma patients in tumor and TISFs, and explored the relationship between characteristic alterations in glioma evolution and targeted therapies, key clinical treatment options, imaging, treatment response.

Results: We validated the representativeness of TISF circulating tumor DNA (ctDNA) to the tumor genome, 100% (33/33) of the mutations detected in the recurrent tumors were detectable in the TISF samples. there was a significant correlation between recurrent tumors variant allele frequencies (VAFs) and the TISF ctDNA VAFs (R^2= 0.9029, 0.9189). In addition, TISF ctDNA is associated with glioma progression and prognosis. The significant alterations observed after tumor progression were KIT (P = 0.0156), NF1 (P = 0.0078), TSC2 (P = 0.0313), FAT1 (P = 0.0313), SMO (P = 0.0313), RTK/RAS/PI3K pathway (P = 0.0028) and MMR gene (P = 0.0234). And we captured the glioma genomic landscape real-time in vivo and found a complete subclonal selection process of PDGFRA, CDKN2A and mismatch repair gene related mutations which were suggested to be actionable for targeted agents. We also identified the progressively increased number and proportion of temozolomide-related C>T/G>A transitions in glioma genome under temozolomide treatment. These key genetic alterations are associated with clinical progression confirmed on imaging, suggesting their driving role for tumor recurrence and the significance to precise therapy.

Conclusions: Increased TISF ctDNA were associated with disease progression and prognosis. Serial ctDNA testing identified progression alterations. Longitudinal ctDNA evaluation could monitor tumour genomic evolutionary patterns and guide precision medicine.

Introduction

Twenty years of molecular research have identified major genetic changes in human glioblastoma (GBM) (1). The Cancer Genome Atlas (TCGA) provides a more detailed picture of the genetic landscape of untreated glioma(2). These researches confirmed the driver genes and the clinical subtype classification. But the molecular events associated with recurrence is a problem that urgently needs to be clarified. Based on this requirement, the Glioma Longitudinal Analysis (GLASS) has established the evolutionary molecular characteristics of adult diffuse gliomas by DNA sequencing on a large cohort of primary and recurrent glioma pairs(3). The large differencne between the primary and recurrent tumors suggests that the evolution of glioma is highly dynamic and individualized at the molecular level, involving the activation or inhibition of numerous signaling pathways. However, the actual molecular trajectory in vivo between initial and recurrent tumors is still unclear, which is important for real-time knowledge of the

glioma molecular landscape and longitudinal analysis of molecular targets with clinical significance. More importantly these studies face an inevitable problem: due to the spatial heterogeneity within the tumor, Genomes of excised surgical specimens differ from residual lesions, which represents the “missing link” between the primary tumour and recurrent disease(4).

Actually, the above studies clarify the reason for the failure of current targeted therapies, which were formulated on the basis of the molecular pathology in resected tumors, and static molecular targets may be lost in the dynamic recurrence process or even not present at all in recurrent tumors due to the heterogeneity of tumors. We need to find new strategies to track the dynamic alterations in the glioma genome.

We've confirmed in our preliminary study that TISF is a reliable source for real-time monitoring of ctDNA(5). Through the dynamic analysis of TISF ctDNA, we observed different types of evolutionary patterns and found changes in clonal evolution and the presence of dominant subclones during glioma recurrence. We have also traced characteristic alterations of the molecular landscape under treatment induction and explored the early warning information of Temozolomide (TMZ) induced extensive mutations. These important alterations in the glioma genome have significant implications for real-time assessment of tumor progression and guidance of precision therapy.

Materials And Methods

Patient characteristics and ethics statement.

This study retrospectively analyzed tissue samples and TISF samples from patients treated at Henan Provincial People's Hospital from July 2016 to January 2021. All patients received the maximum safe range of surgical treatment and postoperative adjuvant therapy, a reservoir capsule under the scalp was implanted intraoperatively for postoperative care. During the follow-up period, no patient developed complications related to reservoir capsule.

Sample collection.

As we described elsewhere (5). A small amount of TISF (0.5-2ml) was extracted from the implanted reservoir during postoperative clinical courses of glioma in 23 patients (This procedure is clinically non-invasive and uninjurious. Blood samples (5ml) for germline DNA control from each patient were also obtained. Fresh tumor tissues or unstained paraffin-embedded tumor tissues (UPETT) were collected for comparing analysis with TISF ctDNA for every patient. TISF samples analyzed in this study were collected after tumor resection. Tumor tissue samples were collected at a minimum of three loci to avoid errors due to spatial heterogeneity within the tumor. Notably, the TISF 2 sample from Patient 5 and the TISF 2 sample from Patient 11 were cerebrospinal fluid. We demonstrated in a previous study that cerebrospinal fluid and TISF are similar in genetic landscapes, especially when tumors touching to the cerebrospinal fluid space like in Patient 5 and Patient 11(6).

Isolation of cell-free DNA and genomic DNA.

EDTA tubes containing 0.5–2 ml TISF or 5 ml whole blood were centrifuged at 1900 g for 10 minutes. Then, the supernatants from these liquid samples were centrifuged at 16,000 g for additional 10 minutes. After that, samples were stored at 80°C before isolation. Cell-free DNA was extracted from liquid samples using the MagMAX. CellFree DNA Isolation Kit (ThermoFisher Scientific; Waltham, MA, USA) while glioma genomic DNA was extracted from fresh tumor tissue or UPETT with the QIAamp DNA Tissue & Blood Kit (Qiagen; Germantown, MD, USA). Finally, all separated DNAs were quantified using the Qubit 2.0 Fluorometer with the Qubit dsDNA HS Assay kit (Life Technologies; Carlsbad, CA, USA).

Targeted capture and sequencing.

the isolated DNA was cut into 150– 200 bp fragments using Covaris M220 Focused-ultrasonicator. Instrument (Covaris; Woburn, MA, USA). Following the manufacturer's direction to construct Fragmented DNA and ctDNA libraries with the KAPA HTP Library Preparation Kit (Illumina platforms; KAPA Biosystems; Wilmington, MA, USA). The DNA library was captured with a designed panel of 68 genes for brain tumors (GenetronHealth; Beijing, China), these containing major brain tumor-related genes. The DNA sequencing was based on novaseq high-throughput sequencing platform. After sequencing, we adopted such criteria that a mutation had an allele fraction of $\geq 0.1\%$ and a total of ≥ 4 reads were considered existing in liquid samples. Known recurrent loci were further manually checked with Integrative Genomics Viewer (IGV v2.3.34) in the target sample comparing to the normal blood DNA. Using the dbNSFP and the Exome Aggregation Consortium (ExAC) database to exclude either benign mutations with pp2_hdiv score < 0.452 or polymorphic nonsynonymous mutations sites. At the end, all detected mutations were annotated for genes using ANNOVAR, Oncotator and Vep.

Statistical analysis.

PFS and OS were evaluated by log-rank test. Using Cox risk proportional hazard models to evaluate the association of TISF ctDNA with PFS. P-values were calculated using Wald test. Correlation between tissue shared mutations and TISF shared mutations was analyzed by linear regression. VAFs between TISF samples was compared by Mann-Whitney (rank sum) test. We compared the changes in VAF and NOA between progressive and non-progressive patients using the Mann Whitney test. Analysis between paired samples was performed using the wilcoxon rank-sum test. All statistical tests were two-sided, and P values < 0.05 were considered significant. Unless otherwise specified, Prism 8 (Version 8.0.2) and SPSS (Version 22) were used for all analyses.

Results

Classification of glioma patients

We collected 35 tumor samples and 87 TISF samples from 32 glioma patients and performed tumor DNA or TISF ctDNA sequencing. At least one mutation was detected in all of samples. The high positive rate was consistent with our previous research work(5). All patients had at least two TISF samples collected. We assessed the tumor status between two adjacent TISF collections according to RENO criteria. Patients 1–14 experienced tumor progression (disease progression, PD) during surveillance. Patients 24–32 experienced tumor stabilization (including disease stabilization SD, partial remission PR, and complete remission CR) during surveillance. And patients 15–23 experienced tumor stabilization and progression phases successively. Patients were divided into progressive or non-progressive groups according to their imaging performance, and the relevant clinical characteristics are shown in Table 1. In addition to standard chemotherapy, Patient 1,8,10,14,15,23 received bevacizumab (BEV) after tumor recurrence, and patient 2 received apatinib during postoperative radiotherapy.

Table 1
clinical characteristics

Characteristic	Progression(N = 23)	without progression(N = 18)
Age (y); median (range)	51.74(21–78)	52.61(26–78)
Sex, n (%)		
Male	15(65.2)	10(55.6)
Female	8(34.8)	8(44.5)
Histopathology, n (%)		
Glioblastoma, IDH-wild	12(52.2)	12(66.7)
Astrocytoma, IDH-mutant	6(26.1)	3(16.7)
Oligodendrocytoma, IDH-mutant	5(21.7)	3(16.7)
WHO grade, n (%)		
IV	13(56.5)	12(66.7)
II &III	10(43.5)	6(33.3)
IDH status, n (%)		
wild type	12(52.2)	12(66.7)
mutant type	11(47.8)	6(33.3)
Aftertreatment, n (%)		
Chemoradiotherapy	10(43.5)	9(50.0)
Chemotherapy	13(56.5)	9(50.0)
Location, n (%)		
Frontal lobe	7(36.4)	6(33.3)
Temporal lobe	8(43.2)	7(38.9)
Parietal lobe	6(11.4)	5(27.8)
Midline	1(4.5)	0(0.0)
Cerebellum	1(4.5)	0(0.0)

TISF ctDNA reflects the tumour genomic alterations

To clarify whether ctDNA testing of TISF can accurately reflect genomic alterations in tumors, We compared recurrent tumor samples from two patients who underwent secondary surgery and had TISF samples collected before secondary surgery. Patient 10 and Patient 16 collected TISF samples 9 days and 1 day before surgical resection of the recurrent tumor, respectively. We found that 100% (33/33) of the mutations with variant allele frequency (VAF) > 5% found in the recurrent tumors were detectable in the TISF samples (Fig. 1a and 1c). More importantly, there was a significant correlation between recurrent tumors VAFs and the TISF ctDNA VAFs (R^2 = 0.9029, 0.9189) (Fig. 1b and 1d). At the same time, it has been demonstrated in large sample paired tumor studies that most initial gliomas (85%) have clonal structures that persist into recurrence (7). We further analyzed the similarity of trunk clonal structures in paired initial tumors and subsequent TISF samples from patients with four or more shared mutation pairs (VAF > 5%). Correlation analysis of three paired samples from Patient 10 and Patient 12 suggested that ctDNA in TISF provided similar clonal structural information to the initial tumor (R^2 = 0.3882, 0.6309, 0.9807). These data suggest that TISF ctDNA can provide information on the subclonal genomic structure of gliomas.

TISF ctDNA is associated with tumor progression

We compared mutations in TISF before tumor progression or stabilization (baseline) with those after tumor progression or stabilization (PN) (if patients had multiple tumor progression or stabilization, only the last one was counted). The highest VAF detected in each TISF was selected as the representative VAF. Among progressive patients (Patients 1–23), between baseline and PN, paired sample analysis showed an increase in VAF in 16 patients and a decrease in VAF in 7 patients. the mean increase in VAF was 7.9% (194%), which was statistically significant (P = 0.0114, Fig. 2a). Between baseline and PN, paired sample analysis showed an increase in NOA in 20 cases and a decrease in NOA in 3. The mean increase in NOA was 19 (235%), which was statistically significant (P = 0.0065; Fig. 2b).

The correlation between TISF ctDNA and tumor was more pronounced when progressive patients were compared with non-progressive patients (Patients 15–32). At baseline, we observed no difference in VAF and NOA between progressive and non-progressive patients (P = 0.7097, P = 0.3923; Fig. 2c, Fig. 2d). However, at PN, VAF and NOA were significantly higher in progressive patients (P = 0.0100, P = 0.0103; Fig. 2e, Fig. 2f). In addition, when comparing ctDNA changes in individual patients, a significant decrease in VAF and NOA was observed in non-progressive patients (P = 0.0086, P = 0.0005; Fig. 2g, Fig. 2h). In conclusion, these data suggest a correlation between TISF ctDNA and tumor progression.

TISF ctDNA levels affect patient prognosis

We analyzed patients' progression free survival (PFS) and overall survival (OS) based on pre-progression (baseline) TISF ctDNA. The 23 patients who showed tumor progression during the monitoring period were divided into high VAF group (VAF < 1%) and low VAF group (VAF ≥ 1%) according to median VAF, and high NOA group (NOA ≥ 4) and low NOA group (NOA < 4) according to median NOA. PFS and OS were calculated using baseline as the starting point, and PFS and OS were longer in patients with low VAF glioma compared to patients with high VAF glioma (P = 0.0004, P = 0.0035; Fig. 3a, Fig. 3b). On the other

hand, patients with low-NOA glioma had longer survival compared to patients with high-NOA glioma (P = 0.0008, P = 0.0024; Fig. 3c, Fig. 3d).

We further performed univariate and multivariate analyses using Cox risk proportional hazard models to evaluate the association of TISF ctDNA with PFS. Univariate Cox analysis suggested that elevated VAF and NOA were associated with worse PFS (HR = 1.054, 95% CI: 1.019–1.091, P = 0.002; Fig. 3e) & (HR = 1.020, 95% CI: 1.004–1.036, P = 0.013; Fig. 3e). In addition, we investigated the effect of age, IDH mutation, MGMT methylation and WHO grade on prognosis. Next, we investigated the effects of IDH mutation, WHO grade, NOA and VAF on prognostic factors in patients in a multivariate Cox model. The results confirmed that VAF and NOA were associated with survival independently of these prognostic factors in patients with glioma (HR = 1.057, 95% confidence interval 1.015-1.100, P = 0.007; Fig. 3e) & (HR = 1.017, 95% confidence interval 1.001–1.033, P = 0.037; Fig. 3e).

To investigate the sensitivity and specificity of VAF and NOA in TISF ctDNA as predictive biomarkers of prognosis for patients with glioma, we generated receiver operating characteristic curves (ROC) using median PFS (282 days) as benchmark. The area under the curve for VAF was 0.803 (95% confidence interval 0.603-1.000; Fig. 3f) and for NOA was 0.792 (95% confidence interval 0.603–0.980; Fig. 3f). Overall, these survival analyses suggest that TISF ctDNA is associated with survival in glioma patients, and therefore is predictive as a biomarker.

Alterations in critical genes and pathways of the population

The above results suggest that elevated TISF ctDNA are associated with glioma progression and worse prognosis. To further explore the specific alterations in TISF ctDNA in glioma recurrence, we compared individual genes before and after tumor progression in the progressive patient population (Patients 1–23) and observed significant changes in NOA between baseline and PN for the following genes, including KIT (P = 0.0078), NF1 (P = 0.0015), TSC2 (P = 0.0313), FAT1 (P = 0.0195) and SMO (P = 0.0313). The changes in NOA across time points for KIT, NF1, TSC2, FAT1 and SMO are shown in Figure S1a-S1e.

When shifting the perspective to changes in the signaling pathway, we observed an average increase in NOA for RTK/RAS/PI3K from baseline and PN (average increase 7.17), with paired analysis showing significant changes in RTK/RAS/PI3K between the two time points (P = 0.0005, Figure S1h). While no statistically significant alterations were found in other glioma classical pathways, such as TP53 signaling pathway (P = 0.7925), RB1 signaling pathway (P = 0.1719).

Other notable changes were in the mismatch repair genes (MMR), including MLH1, MSH2, MSH6 and PMS2, which all showed a mean increase between baseline and PN (average increase 1.39), with statistically significant changes in paired analysis (P = 0.0234, Figure S1i).

Longitudinal analysis of individual glioma evolutionary characteristics

The altered genomic landscape of the population suggests genetic selection for glioma recurrence. We further analyzed the tumor evolutionary trajectory of 23 progressive patients longitudinally from an individual perspective, and the results suggest that there is a genetic correlation and heterogeneity between recurrent and initial tumors. We detected a total of 107 mutations in the initial tumors, with an average of 4.65 mutations. Of these, 54 mutations (50.47%) were detectable in TISF samples, and the shared mutations in WHO □-□ glioma mainly are trunk mutations, including IDH (100%), TP3 (87.5%), ATRX 37.5%, PIK3CA (25%). Shared mutations in WHO grade IV gliomas include PTEN (42.9%), TP3 (28.6%). We detected a total of 660 mutations in TISF samples (only the final TISF samples were counted in patients with multiple TISF samples), with an average of 28.70 mutations. Notably, VAF of shared mutations was much higher than VAF of private mutations in both the initial tumor and TISF ($P = 0.0025$, $P < 0.0001$). This suggests that shared mutations, as the "bridge" between the initial and recurrent tumors, are the main cause of tumorigenesis and recurrence at the population level, while most other private mutations are probably just "bystanders". However, private mutations with high VAF values were found in the TISF of some patients, in particular, the appearance of these private mutations was temporally related to tumor progression. We identified those private mutations as de novo dominant subclonal mutations and divided the patients into three groups by the ratio of the highest VAF of private mutations to the highest VAF of shared mutations in TISF (private/share): the "trunk" group included 5 patients with recurrent tumor genomes dominated by trunk mutations (private/share = 0-0.283). The "subclone" group consisted of 10 patients with recurrent tumor genomes containing subclonal mutations with high VAF values (private/share = 0.341–51.4), and we infer that the dominant subclonal mutations might be involved in tumor recurrence. The "naive" group was the 8 patients without shared mutations. Although further comparison of progression-free survival (PFS) between the groups did not reveal significant differences ($P = 0.8305$), we infer that the "trunk" and "subclonal" groups represent two patterns of glioma recurrence.

Trunk mutations cause tumor recurrence

As described above, the genomes of the recurrent tumors in the " trunk" group included Patient 11, 8, 2, 19, and 9 which were dominated by trunk mutations. Patients 11 had the same mutational profile in TISF as the initial tumor, while Patients 2, 9, 19 and 8 developed de novo mutations, but the private/share was low, 0.091, 0.283, 0.051, 0.032 and 0.018, respectively. The typical case was Patient 8, who underwent surgery and had a pathological diagnosis of glioblastoma, WHO grade IV. Recurrence was soon observed on imaging after 132 days (Fig. 4a). Only *BRAF:p.V600E* and *HIST1H3C:p.K37M* present as shared mutations between the three TISF samples and the initial tumor sample. In particular, we found only this two shared mutations with high VAF in TISF 3 samples sampled at recurrence (*BRAF:p.V600E*/54.5% and *HIST1H3C:p.K37M*/35.4%, Fig. 3b), and other de novo mutations consistently had VAF ≤ 1% in all samples. This suggests that recurrent tumors have the same driver mutations as the initial tumors. Notably the NCCN clinical practice guidelines in Oncology: Central Nervous System Cancers (v1.2021) recommend the use of BRAF/MEK inhibitors for glioblastomas carrying the *BRAF:p.V600E* mutation: dabrafenib/ trametinib, and vimofenib/Cobimetinib as relapse therapy (Class 2A recommendation).

We collected 4 samples in patient 11, including 2 tumor tissue samples and 2 TISF samples. The pathological diagnosis of this patient was: astrocytoma, WHO grade II (Fig. 4c). The genetic profile during tumor progression in Patient 11 was identical (Fig. 4d) which suggest that glioma grew in exactly the same pattern. In addition we show the heat map of other patients in the "trunk" group in Figs. 4e to 4h.

Patients with tumor recurrence induced by trunk mutations have a relatively simple mutation in the evolutionary history of the tumor, and this type of tumor has driver mutations that account for the bulk of the tumor, which also means that targeted therapy targeting the driver mutation is expected to produce promising results

Analysis of TISF ctDNA reveals clonal evolution of glioma in vivo

The VAF value of de novo mutations was significantly higher in the "subclonal" group than in the "trunk" group, suggesting subclonal selection in recurrent tumors of "subclone" group. The comparison of dominant subclonal mutations with trunk mutations is shown in Table 2. In addition, we further compared the imaging presentation and treatment strategy with genomic alterations from longitudinal collected TISF samples. The results suggest that the emergence of dominant subclones represents elevated tumor malignancy and treatment resistance, and was related to tumor progression.

Table 2
Dominant subclonal mutations and shared mutations in the "subclonal" group

Patient no.	Shared mutations/VAF%	Dominant subclonal mutation/VAF%	Private/ Share
18	TP53:p.R248W/0.7	NOTCH1:p.F937L/10.7	15.286
12	TP53:p.E258K/78.8	MSH2:p.Q337*/39.3	0.506
10	PDGFRA:p.V658I/49.3	PDGFRA:p.V536E/23.5	0.477
5	PDGFRA:p.E997Q/15.4	MSH6:p.W970*/87.9	5.708
16	ATRX:c.5567-2A > G/55.4	ATRX:p.R2059K/26.3	0.475
6	CDKN2A:c.151-1G > T/2.3	GNAQ:p.T96S/15.2	6.609
13	PTEN:p.Y16*/4.1	NF1:p.G1678Efs*3/1.4	0.341
14	TP53:p.I195T/0.5	GNAQ:p.T96S/25.7	51.4
20	BRAF:p.V600E/0.5	KLF4:p.S196L/0.9	1.8
23	SETD2:p.R1543W/6.9	TERT:c.-124C > T/11.3	1.637

Patient 10 was initially diagnosed with multiple lesions in the right frontal lobe and left cerebral peduncle by imaging, then Patient 10 underwent the first surgery to resect the lesions in the right frontal lobe, the pathological diagnosis was diffuse mesenchymal astrocytoma, WHO grade III. We collected TISF 1 samples at 127 days after diagnosis and detected only 5 mutations with VAF less than 1%. This was consistent with the slow progression of the tumour on imaging up to Day 157. 263 days after diagnosis, the patient underwent a second surgical resection of the left cerebral peduncle lesion due to progressive symptoms, TISF 2 and TISF 3 samples were collected preoperatively and postoperatively, respectively (Fig. 5a). The pathology of the left cerebral peduncle lesion was identical to that of the right frontal lobe, suggesting a common origin of the two tumors. Further analysis revealed a large number of subclonal mutations that appeared after the initial tumor in this patient's TISF samples, most of which had significantly lower VAFs compared to trunk mutations and probably faded away. For example: *PMS2 p.E5K* in TISF 1 samples and *PIK3CA p.V346E* in TISF 2 samples, which were detected with very low VAF values in only one TISF sample and disappeared at the next sample (Fig. 5b). In addition, we also observed that some subclonal mutations did not disappear during tumor progression and their load increased further to near or above the trunk mutation. For example, *PDGFRA:p.V536E* and *CDKN2A:p.L16Pfs*9* mutations in TISF 2 and TISF 3 samples (Fig. 5b). *PDGFRA:p.V536E* VAF increased from 5.6–23.5%. In particular, *PDGFRA:p.V536E* is an activating mutation and can overactivate RTK/RAS/PI3K pathway (8). The *CDKN2A:p.L16Pfs*9* mutation is a frame shift mutation, and its VAF increases from 2.0–19.3%. The frame shift mutation from the 16th amino acid is likely to cause severe damage to protein function. And this further would cause activation of cell cycle protein-dependent kinase, leading to tumor cell growth and proliferation(9). Meanwhile the tumor load increased rapidly on imaging after the second surgery. This suggests a correlation between the appearance of these dominant subclones and tumor progression.

In addition, *MLH1:p.S627F* and *MSH2:p.Q337** in Patient 12 and *MSH6:p.w970** in Patient 5 also showed an increased load (Fig. 6). In particular, the VAF of *MSH6:p.w970** from Patient 5 increased from 26.1% in the TISF 1 sample to 87.9% in the TISF 2 sample, which far exceeded the VAF of the shared mutation *PDGFRA:p.E997Q* and other mutations. What's more, this patient developed intracranial metastases when the TISF 1 sample was obtained, and the tumor growth rate increased in imaging after this period (Fig. 5d). Note that *MSH2:p.Q337**, *MSH6:p.w970** are nonsense mutations, which produce termination codon and cause early termination of protein coding. Whereas MLH1, MSH2 and MSH6 are important components of the MMR, MMR dysfunction is a feature of TMZ resistance(10).

Overall, these dominant subclonal alterations give the corresponding subclonal groups a stronger competitive edge and allow them to gradually dominate the tumor progression and lead to recurrence, malignant progression and distant metastasis, which also suggests the importance of treatment targeting those mutations.

Characteristic molecular trajectory changes under treatment stress

The alkylating agent TMZ is widely used in the treatment of glioma as the prominent treatment for glioma other than surgery. However, the persistence of TMZ-induced O6MeG in DNA can lead to C > T/G > A transitions during DNA replication(10, 11). We defined these C > T/G > A transitions found in TISF samples and not detected in the initial tumor as TMZ-associated mutations, and further investigated the characteristics of these mutations.

As mentioned above, Patient 12 and Patient 5 had TMZ-associated dominant subclonal mutations, and further exploration revealed that the generation of these dominant subclones may be part of the characteristic alterations under TMZ treatment. Patient 12 underwent surgical resection and was diagnosed with oligodendrocytoma, WHO grade III. Prior to the collection of TISF 1 sample, the tumor remained stable, and accordingly, all 33 mutations detected in TISF 1 samples had VAF values less than 1.5%. Thereafter, the tumor load gradually increased on imaging and the overall VAF of TISF 2 was significantly higher than that of TISF 1 (P = 0.004, Fig. 6c). Meanwhile, *MLH 1: p.S627F* and *MSH 2: p.Q337** mutations representing treatment resistance were detected in the TISF 2 sample. Day 161 Patient 10 was treated with BEV, while tumor volume reduction on imaging and decreased mutational load in TISF 3 sample. However, soon thereafter the tumor progressed significantly again and 184 mutations was observed in TISF 4 (Fig. 6b). In addition, except for shared mutations, the proportion of total TMZ-associated mutation VAFs in Patient 10's TISF 1 was 36.3%, while this proportion increased to 99.93% and 96.24% in TISF 2 and TISF 4 samples, suggesting a progressive dominance of TMZ-associated mutations in all de novo tumor mutations (Fig. 5f).

Likewise, Patient 5 underwent surgical resection and was diagnosed with glioblastoma, WHO grade IV. As previously described, this patient had a dominant subclonal mutation of *MSH6:p.W970**, which VAF is 26.1% in the TISF 1 sample, and distant metastases occurred at the time of collection of the TISF 1 sample (Fig. 6d). After that, rapid tumor progression was observed on imaging, with *MSH6:p.W970** mutation VAF reaching 87.9% in the subsequent TISF 2 sample (Fig. 6d and 6e). In addition, the proportion of TMZ-associated mutation VAFs in TISF 1 and TISF 2 were 99.93% and 96.24%, the number of TMZ-associated mutations in TISF 1 and TISF 2 were 188 and 263, respectively. The molecular evolutionary trajectory of these two patients reflected the TMZ-induced features, i.e., a survival advantage of MMR alterations and a progressive increase in the number and proportion of C > T/G > A transition mutations, eventually extensive mutations in the genome occur.

More importantly, in Patient 12's TISF 2 sample there has not yet been an explosion of mutations emerging, but MMR mutations have emerged as the dominant subclone and TMZ-associated mutations account for 99.93% of all mutations. This may be an early warning message of TMZ-induced extensive mutations, because at this time TMZ-associated mutations start to dominate and MMR dysfunction eliminates the opportunity to repair O6MeG-induced mismatches during DNA replication. The subsequent extensive mutations detected in the TISF 4 samples confirmed this conjecture.

Two features were found in TISF samples before and after Patient 12 received BEV: (i) the number of mutations and overall VAF decreased significantly in TISF 3 samples after BEV treatment, and the MMR

dominant subclonal mutations were suppressed. However, TISF 4, which was collected only 4 months after TISF 3, has an explosive increase in the number of TMZ-associated mutations (Fig. 6b and 6f). The reason is presumed to be the continued accumulation of O6MeG in DNA caused by TMZ, and the presence of large amounts of O6MeG could lead to a dramatic increase of de novo mutations; (ii) the dominant subclonal mutations and trunk mutations other than IDH in the TISF 2 samples did not appear in the TISF 3 and TISF 4 samples after BEV treatment (Fig. 6b), which indicates that the tumor clonal structure is changed after BEV application. However, BEV is currently thought to affect the tumor microenvironment rather than the tumor cells and has no effect on overall survival(12). Whether the altered tumor clonal structure comes from the application of BEV remains to be discussed. On the other hand, it also suggests the presence of ancestral clones containing IDH trunk mutations, and this clonal population is resistant to alkylating agent treatment and targeted therapy (13).

Discussion

The recurrence of glioma is highly individualized, especially the presence of subclonal selection is associated with decreased survival in the evolution process(7), and TMZ plays a critical role in driving the transformation of low-grade gliomas to glioblastoma(14). These findings in recurrent glioma samples emphasize the importance of capturing the unique evolutionary trajectory of a single individual and tailoring unique therapeutic regimens. To this end, clinical management requires the development of tools and strategies needed to collect and analyze the molecular evolutionary trajectories of gliomas in real time(4).

Although poorly reported in gliomas, liquid biopsy ctDNA have been extensively studied in other tumors as an assessment factor for disease progression, even if ctDNA alterations predate imaging(15–17). In addition, in a study of metastatic breast cancer, it was demonstrated that higher baseline VAF and NOA predicted a poorer prognosis for patients(18). In gliomas, higher ctDNA concentrations in the early postoperative period were associated with poorer PFS(19). In this study, we report the dynamic changes in TISF ctDNA collected during the progression of glioma. The results suggest that VAF and NOA are significantly increased during tumor progression and are particularly apparent when compared to non-progressive patients. In addition, TISF ctDNA is valuable as a predictive biomarker for the prognosis of glioma patients. Our study argues that TISF ctDNA is associated with glioma progression and prognosis from multiple perspectives, which provides a new tool for clinical disease surveillance and decision making.

To identify specific altering factors of TISF ctDNA in tumor progression. We examined alterations in the population genomic landscape and identified several significant changes following tumor progression, including KIT, NF1, TSC2, FAT1, SMO, and RTK/RAS/PI3K pathways. KIT, NF1, and TSC2 are all located in the RTK/RAS/PI3K pathway, suggesting that KIT, NF1, TSC2, and RTK/RAS/PI3K may promote tumor progression by increasing enhanced tumor malignancy or drug resistance. Similarly, the number of mutations in the MMR gene rose significantly after progression, which is consistent with the long-standing understanding of TMZ treatment in the glioma research community(20).

Furthermore, we followed in vivo the evolution of spatiotemporal heterogeneity in 23 glioma patients to explore the true course of glioma evolution. Analysis of molecular profiles showed that the evolution of glioma is a highly individualized process. On the one hand, gliomas can relapse simply by trunk mutations, such as the genome is stable during tumor progression in patient 8 and patient 11; On the other hand gliomas can undergo subclonal selection by natural selection or treatment induction. For example, dominant subclonal mutations were identified in consecutive samples in Patient 10, 12 and 5. These dominant subclonal mutations, as part of the numerous de novo mutations in gliomas after surgery, invariably provided a stronger competitive edge to the corresponding subclonal populations and contributed to their dominance in the tumor population, this was a process that promoted tumor recurrence and was also verified temporal correlation on imaging. This illustrates an evolutionary pattern common to both LGG and GBM gliomas: during glioma progression, tumors may generate new subclonal somatic mutations either randomly or under chemical induction. Most of de novo mutations not contributing significantly to tumor growth, remaining in the tumor tissue at a low load and possibly fading away. When certain somatic mutations appear and confer higher proliferation, drug resistance or malignancy to the tumor cells, the subclonal population containing these mutations has a relative survival advantage and dominates the entire subclonal cluster of tumors, making treatment less effective and accelerating recurrence. This competitive relationship is consistent with Darwinian evolutionary theory, and the fate of a clone is governed by survival of the fittest(21). Evolutionary studies of metastatic tumor samples also confirm the existence of this evolutionary pattern(22). Our study confirms this evolutionary pattern in gliomas in human body, and the presence of characteristic TMZ-related molecular trajectories provides a predictable direction for this evolution

Incorporating evolutionary dynamics into the elaboration of therapeutic protocols may significantly extend the duration of disease control with existing drugs(22). Whether for immune evasion, treatment resistance or higher proliferative activity, dominant mutations, as adaptive alterations in tumors at this stage, are promising as precise targets for current targeted therapies. In our study, the *PDGFRA p.V536E* mutation of Patient 10 was found to be highly sensitive to the inhibitory effect of imatinib, despite imatinib has failed to improve survival of glioblastoma patients (8). For the MMR mutations in Patient 12 and 5, it has been shown that tumors with MMR defects are sensitive to nitrosourea lomustine (20). Continuous TISF analysis enables the identification of dominant subclones of glioma in real time and brings a new direction to the clinical treatment strategy of glioma. Benefiting from TISF that can be accessed non-invasively in real time, we have the opportunity to make timely clinical decisions in response to the emergence of dominant subclones.

Mehdi et al. identified an association between TMZ treatment, MMR alterations, and the occurrence of hypermutations through mutational analysis of 10,294 glioma samples, which suggested a promising means of prevention(20). In this study, we observed a characteristic alteration under TMZ treatment and the entire process of TMZ-induced extensive mutations, in which the number and proportion of C > T/G > A transitions gradually increased and a survival advantage was observed for subclones with altered MMR genes. Extensive research evidence also suggests that TMZ-associated mutations drive tumor progression through multiple pathways, which emphasizes the importance of balancing the initial

antitumor effects and mutagenic capacity of TMZ(14). Fortunately, we have identified possible early warning signals of TMZ-induced extensive mutations through dynamic monitoring, and making countermeasure treatment at this critical point is expected to reduce the occurrence of hypermutations. Our research results also provided a way to monitor treatment response. However, future studies with larger cohorts are needed to clarify the specific timing of intervention and further develop standard treatment protocols.

There is a limitation to our study, we found alterations of the glioma genome and their relation with precision medicine by TISF ctDNA analysis, which has opened the door to a new field of glioma research. However, to a broader view, liquid biopsy has the potential to monitor tumour cells, cell- free RNAs (mRNAs, long non- coding RNAs and microRNAs), extracellular vesicles, proteins and metabolites that originates from tumors and can reflect tumor status from multiple perspectives(23). This shows us a broad research prospect, and the current study on TISF ctDNA is only a foundation. Future studies of multiple tumor-derived materials extracted from TISF will construct the biological behavior of gliomas in real time at multiple levels. In addition, although we have taken multi-locus sequencing of tumor samples and confirmed that TISF can represent current recurrent tumor samples, there is still broader heterogeneity to be discussed. For example, tumor cells at the tumor infiltrating margins and SVZ region have been demonstrated to arise early during tumour growth and to be a key factor for tumor treatment resistance and implant regeneration (13). Furthermore there may be unmonitored heterogeneity within the tumor mass. Therefore TISF combined with multiple types of samples is a direction to further refine molecular monitoring of glioma.

We have revealed the "real world" of glioma evolution. The emergence of dominant clones and the presence of early warning signs of TMZ-induced extensive mutations indicate the existence of critical points in the evolution of glioma, and it is important to identify and respond to these critical points timely. Our findings provide new strategies and directions for the clinical management of glioma.

Conclusion

This study provides evidence that TISF ctDNA can represent the clonal structure of the tumor genome. Furthermore, we demonstrate that sequential TISF ctDNA testing can detect genomic progression in glioma populations, and increased NOA and MAF correlate with disease progression and prognosis. More importantly, TISF enables real-time knowledge of individualized genomic evolution of gliomas, which include clonal selection and treatment-induced characteristic alterations that correlate with imaging-confirmed clinical progression, and this provides a basis for future precision diagnosis and treatment of gliomas.

Abbreviations

NGS	Next generation sequencing
TMZ	Temozolomide
GBM	Glioblastoma
NOA	Number of alteration
TISF	Tumor in-situ fluid
MTX	Methotrexate
BEV	Bevacizumab
ctDNA	Circulating tumor DNA
VAF	Variant allele fraction
MMR	Mis-match repair
PFS	Progression free survival
OS	Overall survival
ROC	Receiver operating characteristic curve

Declarations

Ethics approval and consent to participate:

Written informed consent was signed by all patients according to the protocol approved by the Henan Provincial People's Hospital Institutional Review Board and Ethics Committee.

Availability of data and materials:

The major data is in the paper and all data relating to the paper will be deposited in a public database and provided for researchers. (We will publish the data sets presented in this study in online repositories after the manuscript is accepted.)

Conflicts of interest:

The authors declare that there is no competing interest.

Funding:

Science and Technology Tackle Program of Henan Province (Grants no. 192102310126) and Joint Project of Medical Science and Technology Tackling Plan of Henan Province (Grants no. 201601016).

Author contribution:

X.B. conceived the study. X.B., K.D. and Z.S. designed and conducted the study. K.D., Z.S. and X.B. performed the analysis. K.D. and Z.S. drafted the manuscript. X.B., A.Z., F.S., J.H., M.L. and T.L. reviewed the design and revised the manuscript. Z.S., J.Y., Y.B., S.W., S.X., Y.G., Z.Y., C.B., Z.C. and J.G. provided clinical specimens and patient data. L.K. performed pathology review. G.L. reviewed the genomic annotation. M.W. performed the imaging review. T.L. and M.W. oversaw the progress of the trial. All authors read and approved the manuscript.

Acknowledgements:

We thank the patients and their families. Thanks to the health Department of Henan Province for supporting this study.

Authors' information:

Department of Neurosurgery, Zhengzhou University People's Hospital, Henan Provincial People's Hospital, Zhengzhou, 450003, China.

Kaiyuan Deng, Zhiyuan Sheng, Sensen Xu, Yage Bu, Shuang Wu, Ziyue Zhang, Guangzhong Guo, Guanzheng Liu, Jinliang Yu, Yushuai Gao, Zhaoyue Yan, Xingyao Bu

Henan Provincial Neurointerventional Engineering Research Center, Henan International Joint Laboratory of Cerebrovascular Disease, and Henan Engineering Research Center of Cerebrovascular Intervention Innovation, Zhengzhou, Henan, 450003, China.

Jianjun Gu, Tianxiao Li

Department of Pathology, Zhengzhou University People's Hospital, Henan Provincial People's Hospital, Henan University People's Hospital, Zhengzhou, 450003, China.

Lingfei Kong

Department of Center for Clinical Single Cell Biomedicine, Clinical Research Center, Department of Oncology, Zhengzhou University People's Hospital, Henan Provincial People's Hospital, Henan University People's Hospital, Zhengzhou, 450003, China.

Gang Liu

Department of Radiology, Zhengzhou University People's Hospital, Henan Provincial People's Hospital, Henan University People's Hospital, Zhengzhou, 450003, China.

Meiyun Wang

Consent for publication:

Not applicable.

References

1. Furnari FB, Fenton T, Bachoo RM, Mukasa A, Stommel JM, Stegh A, et al. Malignant astrocytic glioma: genetics, biology, and paths to treatment. Genes Dev [Internet]. 2007;21:2683–710. Available from: http://www.genesdev.org/cgi/doi/10.1101/gad.1596707
2. Sanchez-Vega F, Mina M, Armenia J, Chatila WK, Luna A, La KC, et al. Oncogenic Signaling Pathways in The Cancer Genome Atlas. Cell [Internet]. 2018;173:321-337.e10. Available from: http://www.ncbi.nlm.nih.gov/pubmed/29625050
3. Narayanan A, Turcan S. The Magnifying GLASS: Longitudinal Analysis of Adult Diffuse Gliomas. Cell [Internet]. 2020;180:407–9. Available from: https://linkinghub.elsevier.com/retrieve/pii/S0092867420300970
4. Spiteri I, Caravagna G, Cresswell GD, Vatsiou A, Nichol D, Acar A, et al. Evolutionary dynamics of residual disease in human glioblastoma. Ann Oncol [Internet]. 2019;30:456–63. Available from: https://linkinghub.elsevier.com/retrieve/pii/S0923753419310725
5. Sheng Z, Yu J, Deng K, Andrade-Barazarte H, Zemmar A, Li S, et al. Characterizing the Genomic Landscape of Brain Glioma With Circulating Tumor DNA From Tumor In Situ Fluid [Internet]. Front. Oncol. . 2021. page 918. Available from: https://www.frontiersin.org/article/10.3389/fonc.2021.584988
6. Sheng Z, Yu J, Deng K, Bu Y, Wu S, Xu S, et al. Integrating real-time in vivo tumour genomes for longitudinal analysis and management of glioma recurrence. Clin Transl Med [Internet]. 2021;11. Available from: https://onlinelibrary.wiley.com/doi/10.1002/ctm2.567
7. Barthel FP, Johnson KC, Varn FS, Moskalik AD, Tanner G, Kocakavuk E, et al. Longitudinal molecular trajectories of diffuse glioma in adults. Nature [Internet]. 2019;576:112–20. Available from: http://www.nature.com/articles/s41586-019-1775-1
8. Velghe AI, Van Cauwenberghe S, Polyansky AA, Chand D, Montano-Almendras CP, Charni S, et al. PDGFRA alterations in cancer: characterization of a gain-of-function V536E transmembrane mutant as well as loss-of-function and passenger mutations. Oncogene [Internet]. 2014;33:2568–76. Available from: http://www.ncbi.nlm.nih.gov/pubmed/23752188
9. Freedberg DE, Rigas SH, Russak J, Gai W, Kaplow M, Osman I, et al. Frequent p16-independent inactivation of p14ARF in human melanoma. J Natl Cancer Inst [Internet]. 2008;100:784–95. Available from: http://www.ncbi.nlm.nih.gov/pubmed/18505964
10. Aasland D, Götzinger L, Hauck L, Berte N, Meyer J, Effenberger M, et al. Temozolomide Induces Senescence and Repression of DNA Repair Pathways in Glioblastoma Cells via Activation of ATR–CHK1, p21, and NF-κB. Cancer Res [Internet]. 2019;79:99–113. Available from: http://cancerres.aacrjournals.org/lookup/doi/10.1158/0008-5472.CAN-18-1733
11. Choi S, Yu Y, Grimmer MR, Wahl M, Chang SM, Costello JF. Temozolomide-associated hypermutation in gliomas. Neuro Oncol [Internet]. 2018;20:1300–9. Available from: https://academic.oup.com/neuro-oncology/article/20/10/1300/4857168

12. Reardon DA, Brandes AA, Omuro A, Mulholland P, Lim M, Wick A, et al. Effect of Nivolumab vs Bevacizumab in Patients With Recurrent Glioblastoma: The CheckMate 143 Phase 3 Randomized Clinical Trial. JAMA Oncol [Internet]. 2020;6:1003–10. Available from: http://www.ncbi.nlm.nih.gov/pubmed/32437507
13. Spiteri I, Caravagna G, Cresswell GD, Vatsiou A, Nichol D, Acar A, et al. Evolutionary dynamics of residual disease in human glioblastoma. Ann Oncol Off J Eur Soc Med Oncol [Internet]. 2019;30:456–63. Available from: http://www.ncbi.nlm.nih.gov/pubmed/30452544
14. Johnson BE, Mazor T, Hong C, Barnes M, Aihara K, McLean CY, et al. Mutational Analysis Reveals the Origin and Therapy-Driven Evolution of Recurrent Glioma. Science (80-) [Internet]. 2014;343:189–93. Available from: https://www.sciencemag.org/lookup/doi/10.1126/science.1239947
15. Ignatiadis M, Dawson S-J. Circulating tumor cells and circulating tumor DNA for precision medicine: dream or reality? Ann Oncol [Internet]. 2014;25:2304–13. Available from: https://linkinghub.elsevier.com/retrieve/pii/S0923753419369145
16. Misale S, Yaeger R, Hobor S, Scala E, Janakiraman M, Liska D, et al. Emergence of KRAS mutations and acquired resistance to anti-EGFR therapy in colorectal cancer. Nature [Internet]. 2012;486:532–6. Available from: http://www.nature.com/articles/nature11156
17. Mohan S, Heitzer E, Ulz P, Lafer I, Lax S, Auer M, et al. Changes in Colorectal Carcinoma Genomes under Anti-EGFR Therapy Identified by Whole-Genome Plasma DNA Sequencing. Horwitz MS, editor. PLoS Genet [Internet]. 2014;10:e1004271. Available from: https://dx.plos.org/10.1371/journal.pgen.1004271
18. Jacob S, Davis AA, Gerratana L, Velimirovic M, Shah AN, Wehbe F, et al. The Use of Serial Circulating Tumor DNA to Detect Resistance Alterations in Progressive Metastatic Breast Cancer. Clin Cancer Res [Internet]. 2021;27:1361–70. Available from: http://clincancerres.aacrjournals.org/lookup/doi/10.1158/1078-0432.CCR-20-1566
19. Yu J, Sheng Z, Wu S, Gao Y, Yan Z, Bu C, et al. Tumor DNA From Tumor In Situ Fluid Reveals Mutation Landscape of Minimal Residual Disease After Glioma Surgery and Risk of Early Recurrence. Front Oncol [Internet]. 2021;11. Available from: https://www.frontiersin.org/articles/10.3389/fonc.2021.742037/full
20. Touat M, Li YY, Boynton AN, Spurr LF, Iorgulescu JB, Bohrson CL, et al. Mechanisms and therapeutic implications of hypermutation in gliomas. Nature [Internet]. 2020;580:517–23. Available from: http://www.nature.com/articles/s41586-020-2209-9
21. Parker TM, Henriques V, Beltran A, Nakshatri H, Gogna R. Cell competition and tumor heterogeneity. Semin Cancer Biol [Internet]. 2020;63:1–10. Available from: https://linkinghub.elsevier.com/retrieve/pii/S1044579X18301731
22. Cresswell GD, Nichol D, Spiteri I, Tari H, Zapata L, Heide T, et al. Mapping the breast cancer metastatic cascade onto ctDNA using genetic and epigenetic clonal tracking. Nat Commun [Internet]. 2020;11:1446. Available from: http://www.ncbi.nlm.nih.gov/pubmed/32221288

23. Ignatiadis M, Sledge GW, Jeffrey SS. Liquid biopsy enters the clinic — implementation issues and future challenges. Nat Rev Clin Oncol [Internet]. 2021;18:297–312. Available from: http://www.nature.com/articles/s41571-020-00457-x

Figures

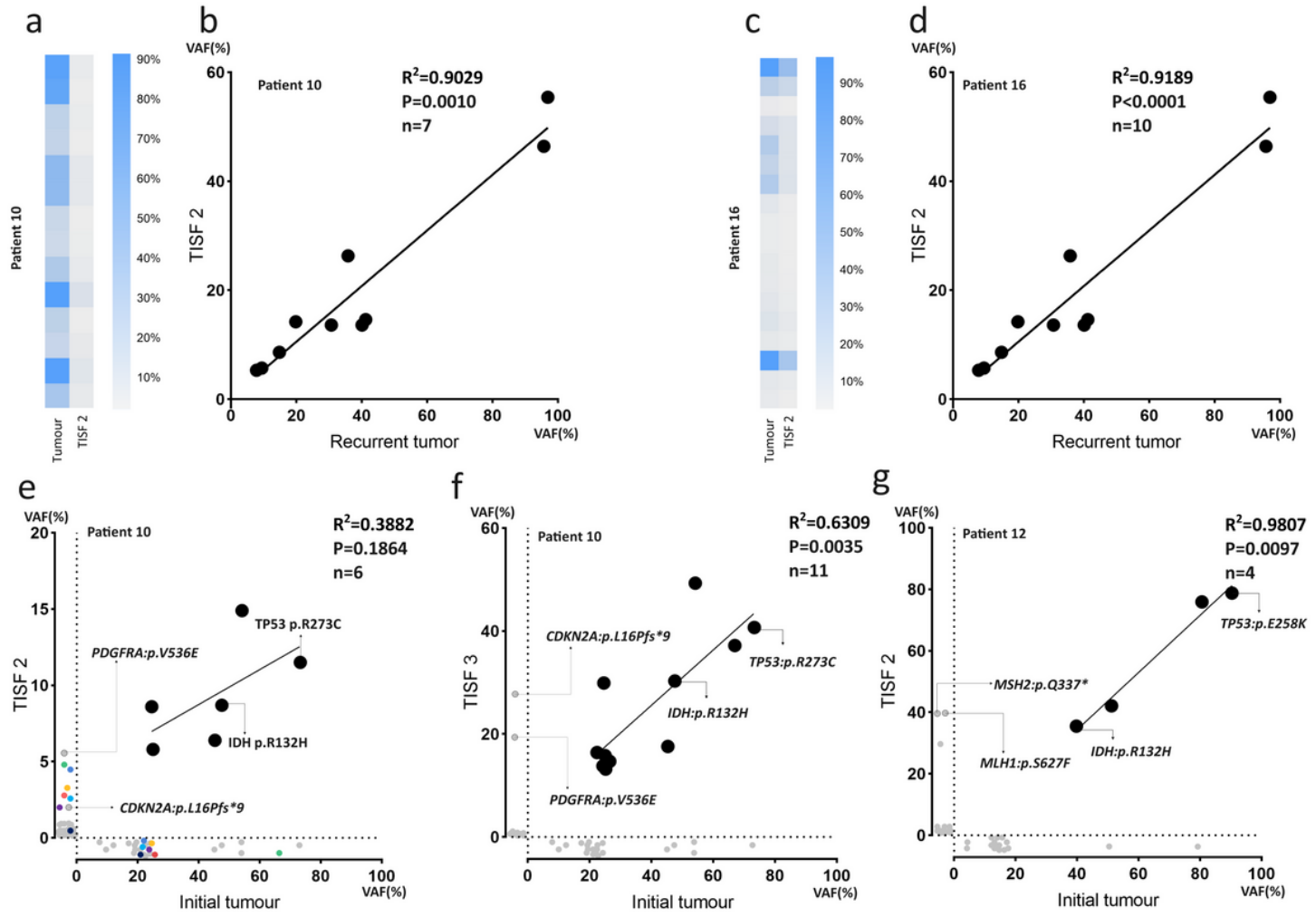

Figure 1

TISF ctDNA reflects the tumour genomic alterations. TISF samples were collected 9 days and 1 day before secondary surgery for Patient 10 and Patient 16, respectively. **a, c** Heat maps show consistency with TISF for shared mutations with VAF≥5% in tumors. **b, d** Correlation of TISF ctDNA VAF with recurrent tumor VAF. Only shared mutations with VAF greater than 5% in both samples were included in the statistics. **e to g** VAF of shared and private mutations in paired initial tumors and TISF samples. Black dots indicate shared mutations, gray dots indicate private mutations, and colored dots indicate shared mutations but VAF does not satisfy >5% in both samples. Linear regression and Goodness-of-fit R^2 indicated in each figure. n, represents the number of shared mutations.

Figure 2

Changes in VAF and NOA at different time points. a, b Progressive patients VAF and NOA at PN versus Baseline; **c, d** Progressive patients versus non-progressive patients VAF and NOA at Baseline; **e, f** Progressive patients versus non-progressive patients VAF and NOA at PN; **g, h** Non-progressive patients VAF and NOA at PN versus Baseline.

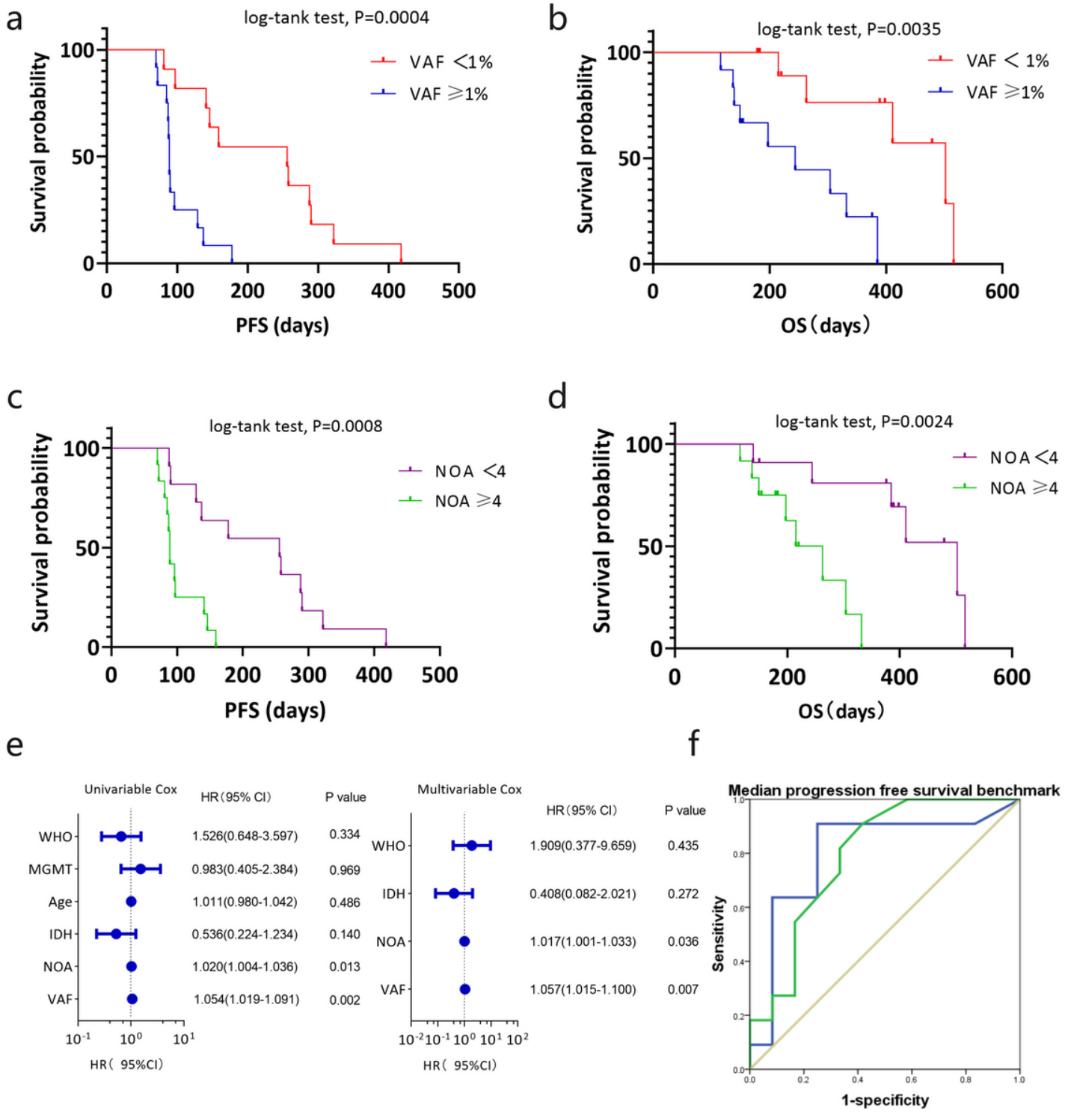

Figure 3

TISF ctDNA can be used as a predictive biomarker for prognosis in patients with glioma. The relationship between baseline VAF and NOA and PFS and OS was described using the Kaplan-Meier method. P-values were calculated using the log-rank test. Patients were classified according to median VAF (**a, b**) and NOA (**c, d**). Both PFS and OS were calculated starting at baseline. **e** Forest plots represent univariate and multivariate survival analyses using Cox proportional hazard models to assess the effect of ctDNA levels and other prognostic variables on survival in patients with glioma, presented as HR (95% CI). P-values were calculated using two-sided Wald test. **f** Sensitivity and 1 -specific ROC curves for glioma patients based on median PFS.

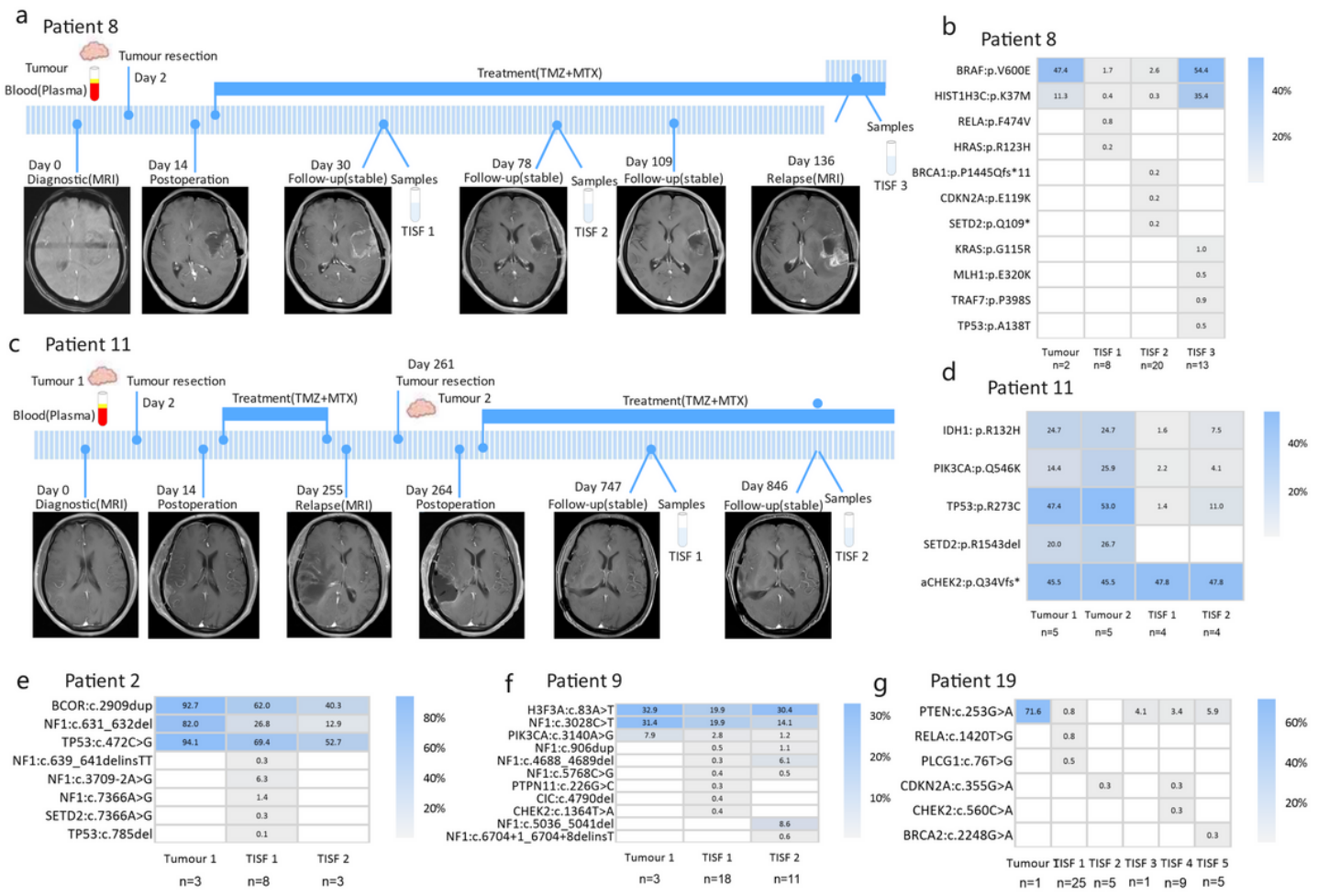

Figure 4

Continuous TISF ctDNA monitoring reveals tumor recurrence caused by trunk mutations. a, c Clinical course of Patient 8 and Patient 11, including tumour surgery, treatment protocol, radiologic images (MRI), sample acquisition time. **b, d, e to g** Heatmap representing mutations and VAFs (%) identified from tumour DNA and TISF ctDNA samples. All shared mutations and some private mutations (with relatively high VAF or proven significant driver) are shown. Hereditary mutations aCHEK2: p.Q34Vfs*42, which

maintained stable VAF values, were identified in both tumor samples and TISF samples from Patient 11. methotrexate (MTX). n represents the number of mutations.

Figure 5

TISF ctDNA analysis reveals clonal selection in the evolution of glioma. a Clinical course of Patient 10, including tumour surgery, treatment protocol, radiologic images (MRI), sample acquisition time. **b** Heatmap representing mutations and VAFs (%) identified from tumour DNA and TISF ctDNA samples. n represents the number of mutation sites. All shared mutations and some private mutations (with relatively high VAF or proven significant driver) are shown. Red frames mark the progression of *PDGFRA p.V536E* and *CDKN2A p.L16Pfs*9* mutations becoming the dominant subclones, consistent with tumor progression on imaging. **c** Distribution of all mutation VAFs in tumour, TISF 1, TISF 2 and TISF 3 samples. There was no statistically difference in the overall mutant VAFs between the TISF 2 and TISF 3 samples (P= 0.1306), but the highest VAF and median VAF of TISF 3 samples were much higher than those of TISF 2 samples (13.50: 0.55; 49.3: 14.9). This indicates that tumor load is elevated at the molecular level, which is consistent with the imaging presentation. Definition of symbols and acronyms: chemoradiotherapy (CRT), methotrexate (MTX). n represents the number of mutations.

Figure 6

TISF reflects the characteristics of treatment-induced mutations. a, d Clinical course of Patient 12 and Patient 5, including tumour surgery, treatment protocol, radiologic images (MRI), and time of sample acquisition. **a** Tumour load remained essentially stable until Day 32, after which it began to gradually increase. A significant decrease of tumor load was confirmed in Day 186 on imaging after BEV treatment, but tumor progressed significantly again after 58 days. **d** Yellow arrows in MRI indicate intracranial metastases of the tumor. **b, e** Heatmap representing mutations and VAFs (%) identified from tumour DNA and TISF ctDNA samples. n represents the number of mutation sites. All shared mutations and some private mutations (with relatively high VAF or proven significant driver) are shown. Red frames mark the progression of *MLH1:p.S627F* , *MSH2:p.Q337** and of *MSH6: p.W970** becoming the dominant subclone. **c** Distribution of all mutation VAFs in tumour, TISF 1, TISF 2, TISF 3 and TISF 4 samples from Patient 12. The difference in overall mutated VAF between TISF 1 samples and TISF 2 samples is statistically significant (P=0.0004). **f** Proportion of TMZ-associated mutations in Patient 12 and patient 5 TISF samples. Proportion of TMZ-associated mutations was calculated by summing the mutation VAFs. This proportion was 36.25%, 99.66%, and 97.63% in TISF 1, TISF 2, and TISF 3 of Patient 12, respectively, and 99.93% and 96.24% in TISF 1 and TISF 2 samples of Patient 5, respectively. This dynamic change suggests a progressive dominance of TMZ-related mutations in de novo mutations. Definition of symbols

and acronyms: chemoradiotherapy (CRT), bevacizumab (BEV), methotrexate (MTX). n represents the number of mutations.

Supplementary Files

This is a list of supplementary files associated with this preprint. Click to download.

- FigS1.png